Published for SISSA by Springer

Received: May 19, 2025
Revised: September 30, 2025
Accepted: November 19, 2025
Published: January 15, 2026

Measurement of $\eta \to \pi^0\gamma\gamma$ branching fraction with the KLOE detector

JHEP01(2026)091

The KLOE-2 collaboration

D. Babusci,[a] P. Beltrame,[b] M. Berlowski,[c,*] C. Bloise,[a] F. Bossi,[a] P. Branchini,[d] B. Cao,[e] F. Ceradini,[f,d] P. Ciambrone,[a] L. Cotrozzi,[b] F. Curciarello,[g,h,1] E. Czerwiński,[i] G. D'Agostini,[j,k] R. D'Amico,[j,k,2] E. Danè,[a] V. De Leo,[j,k,3] E. De Lucia,[a] A. De Santis,[a] P. De Simone,[a] A. Di Domenico,[j,k] E. Diociaiuti,[a] D. Domenici,[a] A. D'Uffizi,[a] G. Fantini,[j,k] S. Fiore,[k,4] A. Gajos,[i] S. Gamrat,[i] P. Gauzzi,[j,k] S. Giovannella,[a] E. Graziani,[d] F. Ignatov,[b] X. Kang,[l] A. Kupsc,[e,c] G. Mandaglio,[m,n] M. Martini,[a,o] S. Miscetti,[a] P. Moskal,[i] A. Passeri,[d] V. Patera,[p,k] E. Perez del Rio,[i] L. Punzi,[q,v] F. Sborzacchi,[a,4] M. Schioppa,[g,h] A. Selce,[a] M. Silarski,[i] F. Sirghi,[a,r] E.P. Solodov,[s,t] T. Teubner,[u] G. Venanzoni,[b,q,u] N. Vestergaard,[b] W. Wiślicki,[c] M. Wolke[e] and E. Zaid[b]

[a] *Laboratori Nazionali di Frascati dell'INFN, Frascati, Italy*
[b] *Department of Physics, University of Liverpool, Liverpool, U.K.*
[c] *National Centre for Nuclear Research, Warsaw, Poland*
[d] *INFN Sezione di Roma Tre, Roma, Italy*
[e] *Department of Physics and Astronomy, Uppsala University, Uppsala, Sweden*
[f] *Dipartimento di Matematica e Fisica dell'Università "Roma Tre", Roma, Italy*
[g] *Dipartimento di Fisica dell'Università della Calabria, Arcavacata di Rende, Italy*
[h] *INFN Gruppo collegato di Cosenza, Arcavacata di Rende, Italy*
[i] *Institute of Physics, Jagiellonian University, Cracow, Poland*
[j] *Dipartimento di Fisica dell'Università "Sapienza", Roma, Italy*
[k] *INFN Sezione di Roma, Roma, Italy*
[l] *School of Mathematics and Physics, China University of Geosciences, Wuhan, China*
[m] *Dipartimento di Scienze Matematiche e Informatiche, Scienze Fisiche e Scienze della Terra dell'Università di Messina, Messina, Italy*
[n] *INFN Sezione di Catania, Catania, Italy*

*Corresponding author.
[1] Present address: ENEA, Centro Ricerche Casaccia, Santa Maria di Galeria, Roma, Italy.
[2] Present address: University of Ferrara, Ferrara, Italy.
[3] Present address: ENEA, Centro Ricerche Frascati, Frascati, Italy.
[4] Present address: CERN, European Organization for Nuclear Research, Geneva, Switzerland.

Open Access, © The Authors.
Article funded by SCOAP[3].

https://doi.org/10.1007/JHEP01(2026)091

[o] *Dipartimento di Scienze e Tecnologie applicate, Università "Guglielmo Marconi", Roma, Italy*
[p] *Dipartimento di Scienze di Base ed Applicate per l'Ingegneria dell'Università "Sapienza", Roma, Italy*
[q] *INFN Sezione di Pisa, Pisa, Italy*
[r] *Horia Hulubei National Institute of Physics and Nuclear Engineering, Măgurele, Romania*
[s] *Budker Institute of Nuclear Physics, Novosibirsk, Russia*
[t] *Novosibirsk State University, Novosibirsk, Russia*
[u] *Department of Mathematical Sciences, University of Liverpool, Liverpool, U.K.*
[v] *Scuola Normale Superiore, Pisa, Italy*

E-mail: Marcin.Berlowski@ncbj.gov.pl

Abstract: We present a measurement of the doubly radiative decay $\eta \to \pi^0\gamma\gamma$ based on a sample of 82 million η mesons produced in the $e^+e^- \to \phi \to \eta\gamma$ process at the Frascati ϕ-factory DAΦNE. From the data analysis, 1246 ± 133 signal events were observed. By normalising the signal to the well-known $\eta \to 3\pi^0$ decay the branching fraction $\mathcal{B}(\eta \to \pi^0\gamma\gamma)$ is measured to be $(0.98 \pm 0.11_{\text{stat}} \pm 0.14_{\text{syst}}) \times 10^{-4}$. This result agrees with a preliminary KLOE measurement, but is a factor of two smaller than the current world average. Results for $d\Gamma(\eta \to \pi^0\gamma\gamma)/dM^2(\gamma\gamma)$ are also presented and compared with the latest theoretical predictions.

Keywords: e^+-e^- Experiments

ArXiv ePrint: 2505.09285

Dedicated to the memory of Giuseppe Fabio Fortugno

JHEP01(2026)091

Contents

1 **Introduction** 1

2 **Detector** 2

3 **Event selection** 3

4 **The normalisation channel** 7

5 **The signal extraction** 8

6 **Systematic studies** 10

7 **Results** 12

1 Introduction

The doubly radiative decay $\eta \to \pi^0\gamma\gamma$ has long been of interest due to the suppression of leading contributions in the effective field theory of strong interactions at low energies — Chiral Perturbation Theory (ChPT). In addition, the process is experimentally challenging to measure, owing to the dominant $\eta \to 3\pi^0$ background. Its branching fraction has been revised downwards several times due to significant background contamination.

The ChPT description includes both tree-level and loop contributions from pseudoscalar mesons, using an expansion in powers of the four-momentum transfer, p, and the quark masses. For the $\eta \to \pi^0\gamma\gamma$ decay, contributions from tree diagrams vanish at both $\mathcal{O}(p^2)$ and $\mathcal{O}(p^4)$, and at one-loop level $\mathcal{O}(p^4)$ terms are strongly suppressed, therefore the first significant term arises at $\mathcal{O}(p^6)$ [1], with the predicted baseline partial decay width of 0.31 eV. However, due to cancellations among the lower-order terms, the $\eta \to \pi^0\gamma\gamma$ decay width is highly sensitive to the details of the calculation and to the model-dependent determination of the coefficients in the expansion of the chiral Lagrangian. Theoretical estimates of the partial decay width within ChPT are provided in refs. [2] and [3]. The value re-evaluated in ref. [4] is $\Gamma(\eta \to \pi^0\gamma\gamma) = (0.33 \pm 0.08)\,\text{eV}$. This corresponds to a branching fraction of $\mathcal{B}(\eta \to \pi^0\gamma\gamma) = (2.54 \pm 0.62) \times 10^{-4}$, using the world average for the total η decay width, $\Gamma_\eta = (1.31 \pm 0.05)\,\text{keV}$ [5]. An alternative description of the process is provided by the Vector Meson Dominance (VMD) model, in which one must account for contributions from tree-level processes, with the vector mesons ρ^0 or ω mediating between the η–γ and π^0–γ vertices. Furthermore, the latest calculation presented in ref. [6] predicts the value of $\mathcal{B}(\eta \to \pi^0\gamma\gamma)$ to be $(1.35 \pm 0.08) \times 10^{-4}$, based on empirical studies using experimentally determined couplings, and $(1.30 \pm 0.08) \times 10^{-4}$ when the couplings are derived from the VMD model. Other recent calculations can be found in refs. [7, 8] (see also the review in ref. [9]).

Experimentally, the $\eta \to \pi^0\gamma\gamma$ decay is difficult to distinguish from background processes. The most precise measurements of $\Gamma(\eta \to \pi^0\gamma\gamma)$ have been reported by the AGS/Crystal

JHEP01(2026)091

Ball [10] and A2/Crystal Ball [11] Collaborations. The partial decay widths were determined to be $(0.285 \pm 0.031_{\text{stat}} \pm 0.061_{\text{syst}})$ eV and $(0.330 \pm 0.030_{\text{tot}})$ eV, respectively. When expressed in terms of the branching fraction, the corresponding values are $\mathcal{B}(\eta \to \pi^0\gamma\gamma) = (2.21 \pm 0.24_{\text{stat}} \pm 0.47_{\text{syst}}) \times 10^{-4}$ and $(2.56 \pm 0.24_{\text{tot}}) \times 10^{-4}$, respectively. These results are in tension with the preliminary measurement from the KLOE Collaboration [12], which reports $\mathcal{B}(\eta \to \pi^0\gamma\gamma) = (0.84 \pm 0.27_{\text{stat}} \pm 0.14_{\text{syst}}) \times 10^{-4}$, based on a data sample of 68 ± 23 events. This earlier result refers to a smaller and independent dataset than the one presented in the current work.

2 Detector

The measurement of the $\eta \to \pi^0\gamma\gamma$ decay was performed using the KLOE detector at the DAΦNE ϕ-factory [13] in Frascati, Italy. DAΦNE is an e^+e^- collider operating at a centre-of-mass energy of 1019.5 MeV, corresponding to the ϕ meson mass. The ϕ mesons are produced almost at rest with respect to the laboratory frame. The total production cross-section at this energy is approximately 3 μb for the $e^+e^- \to \phi$ process. The beams collide at a small crossing angle of about 25 mrad, resulting in ϕ mesons with a transverse momentum of roughly 13 MeV/c. The η mesons are produced via the radiative decay $\phi \to \eta\gamma$, which has a branching fraction of approximately 1.3%. The present measurement is based on an integrated luminosity of 1.7 fb^{-1} collected in 2004 and 2005.

The KLOE detector [14] consists of a large cylindrical drift chamber (DC), 3.3 metres in length and 4 metres in diameter, surrounded by a finely segmented sampling calorimeter (EMC) composed of lead and scintillating fibres. The EMC comprises a cylindrical barrel and two endcaps, providing 98% solid-angle coverage. The entire detector is immersed in a magnetic field of 0.52 T. The beam pipe at the interaction region is spherical in shape, with a radius of 10 cm, and is constructed from a 0.5 mm thick beryllium-aluminium alloy. The DC [15] contains 12,582 drift cells and is filled with a low-density gas mixture of 90% helium and 10% isobutane. Tracks are reconstructed with position resolutions of approximately $\sigma_{xy} \sim 150$ μm in the transverse plane and $\sigma_z \sim 2$ mm along the beam axis. The transverse momentum resolution is $\sigma(p_t)/p_t \sim 0.4\%$. Vertices are reconstructed with a spatial accuracy of approximately 3 mm. The EMC [16] comprises a total of 88 modules, segmented into 2,440 cells with a cross-section of approximately 4.4×4.4 cm^2, arranged in five layers in depth. Each cell is read out at both ends by photomultipliers. The signal amplitudes are used to determine the energy deposited in each cell, while the position along the fibres is determined from the time difference of the signals collected by the two photomultipliers. Hit cells with both time and spatial information consistent with one another are grouped into clusters. The cluster energy, E, is defined as the sum of the energy deposits, while the cluster time, T, and position, R, are energy-weighted averages. The energy and time resolutions are given by $\sigma_E/E = 5.7\%/\sqrt{E\ [\text{GeV}]}$ and $\sigma_t = 57$ ps$/\sqrt{E\ [\text{GeV}]} \oplus 140$ ps, respectively. Cluster positions are measured with a resolution of 1.3 cm in the coordinate transverse to the fibres and 1.4 cm$/\sqrt{E\ [\text{GeV}]}$ in the longitudinal coordinate, derived from timing information. The trigger [17] requires at least two energy deposits in the EMC exceeding thresholds of $E > 50$ MeV for the barrel and $E > 150$ MeV for the endcaps. The higher energy threshold for the endcaps is chosen to reduce machine background, which predominantly contributes

JHEP01(2026)091

at small angles relative to the beam directions. A veto on cosmic particles rejects events with high energy deposits in the outermost layers of the calorimeter, while an offline software background filter, utilising both calorimeter and DC information prior to track reconstruction, further suppresses machine background events [18]. The collected data are divided by an event classification filter [18] into streams corresponding to different categories. These streams are stored in separate files for subsequent analysis.

3 Event selection

The signature of the process $\phi \to \eta\gamma$, with $\eta \to \pi^0\gamma\gamma$, in our measurement consists of five neutral clusters — that is, clusters not associated with tracks — detected in the calorimeter, with a total deposited energy exceeding 0.8 GeV. Since there are no charged particles in the final state, events containing tracks associated to reconstructed clusters are rejected. To suppress machine background, which predominantly affects the signals in the endcaps, clusters are required to have energies of at least 20 MeV and centroids within polar angles between 25° and 155°. Furthermore, a neutral cluster must satisfy the condition $|t - r/c| < \min[5\sigma_t(E), 2\text{ ns}]$, where t is the photon flight time, r is the corresponding path length, c is the speed of light, and $\sigma_t(E)$ is the EMC time resolution for a cluster of energy E. A total of 2.6×10^6 data events with exactly five prompt clusters are selected for the analysis.

The background and signal are estimated using a Monte Carlo (MC) sample generated with ten times the integrated luminosity of the real data. The MC simulation includes both final- and initial-state radiative corrections, incorporates machine background, and accounts for trigger efficiency on a run-by-run basis. The main physics background process is $\phi \to (\eta \to 3\pi^0)\gamma$. Other considered channels include[1] $\phi \to (a_0 \to \pi^0\eta)\gamma$, $\phi \to (f_0 \to \pi^0\pi^0)\gamma$, and $e^+e^- \to (\omega \to \pi^0\gamma)\pi^0$. These processes are generated using the GEANFI MC generator, based on the GEANT simulation package [18], and rely on branching fractions from the Particle Data Group (PDG) as well as cross-sections measured by KLOE [19–23]. Moreover, the $\phi \to (\eta \to 3\pi^0)\gamma$ sample is divided into four categories: a) two photons not detected; b) two photons merged into one cluster; c) one photon lost and one photon merged; d) other instances not covered by the above categories. The $\eta \to \pi^0\gamma\gamma$ signal is generated according to a phase-space distribution. The preselection efficiencies, evaluated using the signal MC sample after the initial 5γ selection, are 48% for the signal and 9% for the sum of the backgrounds. The background yield after preselection is given in the third column of table 1.

A 9-constraint (9C) kinematic fit is applied to improve the resolution of the reconstructed clusters. The constraints include total energy and momentum conservation, under the assumption that all clusters originate from photons. The free parameters in the fit are the cluster positions, energies, and times of flight for all five photons, as well as the energies of the e^+ and e^- beams, and the average position of the e^+e^- interaction point. A requirement on the kinematic fit probability — greater than 10% — removes approximately 90% of background events, which typically involve undetected particles or additional energy from machine background, while retaining 87% signal efficiency, as illustrated in figure 1. The

[1]Throughout this paper, a_0, f_0, and ω refer to $a_0(980)$, $f_0(980)$, and $\omega(782)$, respectively.

JHEP01(2026)091

Background channel	Generated (10^6)	Preselected (10^6)	Final (10^3)
$\phi \to (\eta \to 3\pi^0)\gamma$:			
2 lost	—	1.0	29.0
1 lost 1 merged	—	0.03	11.9
2 merged	—	0.4	1.0
other cases	—	0.07	3.2
$\phi \to (\eta \to 3\pi^0)\gamma$ sum	21.8	1.5	45.2
$\phi \to (a_0 \to \pi^0\eta)\gamma$	0.18	0.08	1.7
$\phi \to (f_0 \to \pi^0\pi^0)\gamma$	0.45	0.2	0.3
$e^+e^- \to (\omega \to \pi^0\gamma)\pi^0$	0.82	0.4	1.6
Total contribution	23.2	2.2	48.8

Table 1. Residual backgrounds estimated from MC simulations. Number of events shown at three stages: generated (second column), after preselection (third column), and after all analysis cuts (last column). No entries are present in the "generated" column for the $\phi \to (\eta \to 3\pi^0)\gamma$ categories, as these are defined only after event reconstruction.

distributions of the following variables, after applying the cut on kinematic fit probability, are shown in figure 2:

- $M(\pi^0\gamma\gamma)$, the invariant mass calculated by excluding the photon whose energy is closest to 363 MeV — the expected energy of the recoil photon from the $\phi \to \eta\gamma$ decay;
- $M^2(\gamma\gamma)$, the invariant mass squared of the two photons not associated with the π^0, where the π^0 is defined as the photon pair with an invariant mass closest to the nominal π^0 mass;
- $\theta(\gamma)$, the polar angle of each of the five photon clusters;
- $E(\gamma)$, the energy of each of the five photon clusters.

The background from the $\phi \to (a_0 \to \pi^0\eta)\gamma \to 5\gamma$ process is suppressed using an 11-constraint (11C) kinematic fit with additional requirements. After excluding the photon whose energy is closest to 363 MeV — the expected energy of the recoil photon from the $\phi \to \eta\gamma$ decay — one pair of photons is required to originate from an η meson and the other from a π^0 meson. Among all possible combinations, the one with the lowest χ^2 is selected, and the event is discarded if the fit probability exceeds 10%.

A similar procedure is applied to suppress background processes with $\pi^0\pi^0$ in the final state. In this case, the additional constraints require two photon pairs to originate from π^0 mesons. These events are also rejected if the fit probability is greater than 10%.

To further suppress backgrounds involving neutral pion pairs in the final state, we use a χ^2 variable defined as follows:

$$\chi^2(2\pi^0) = \frac{[M(\gamma_1\gamma_2) - m(\pi^0)]^2}{\sigma^2(\gamma_1\gamma_2)} + \frac{[M(\gamma_3\gamma_4) - m(\pi^0)]^2}{\sigma^2(\gamma_3\gamma_4)}, \tag{3.1}$$

where $M(\gamma\gamma)$ is the invariant mass of a photon pair, $m(\pi^0)$ is the neutral pion mass and $\sigma(\gamma\gamma)$ is the corresponding mass resolution. In our case, the angular uncertainty is negligible

JHEP01(2026)091

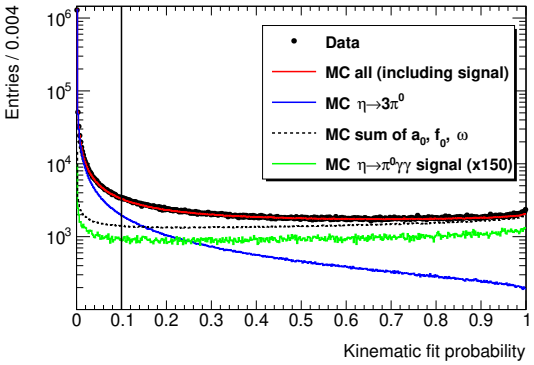


Figure 1. Distribution of the 9C kinematic fit probability. Black points with error bars represent the data. The red histogram shows the sum of all Monte Carlo (MC) contributions, with individual components indicated by coloured lines: blue line — $\eta \to 3\pi^0$ MC; dotted black line — combined MC contributions from a_0, f_0, and ω; green histogram — $\eta \to \pi^0\gamma\gamma$ signal MC sample, scaled up by a factor of 150. The total number of MC events has been normalised to match the data. The black vertical line indicates the applied cut-off value.

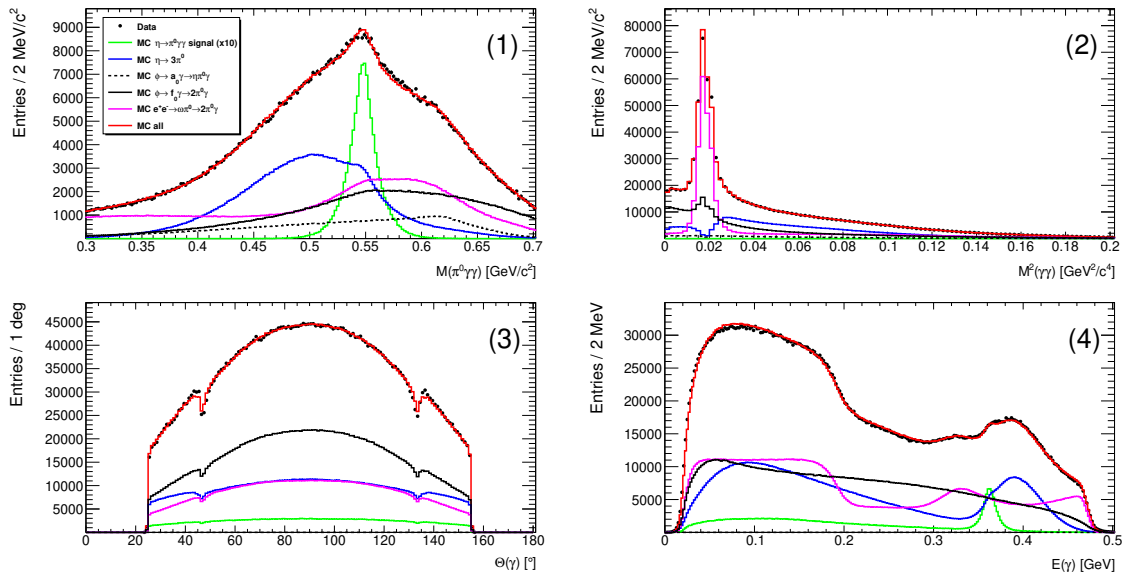


Figure 2. Data-MC comparison of the following distributions after event selection and the cut on the 9C kinematic fit probability: (1) $M(\pi^0\gamma\gamma)$, (2) $M^2(\gamma\gamma)$, (3) $\theta(\gamma)$ and (4) $E(\gamma)$. Black points with error bars represent the data. The red histogram shows the sum of all Monte Carlo (MC) contributions, with individual components represented by coloured lines: blue line — $\phi \to (\eta \to 3\pi^0)\gamma$, black solid line — $\phi \to (f_0 \to \pi^0\pi^0)\gamma$, black dotted line — $\phi \to (a_0 \to \pi^0\eta)\gamma$, magenta line — $e^+e^- \to (\omega \to \pi^0\gamma)\pi^0$, green line — $\phi \to (\eta \to \pi^0\gamma\gamma)\gamma$ signal, scaled up by a factor of 10. The total number of MC events has been normalised to the data. The enhancement in panel (4) around 360 MeV corresponds to recoil photons from the $\phi \to \eta\gamma$ decay.

JHEP01(2026)091

compared to the energy uncertainty, so $\sigma(\gamma\gamma)$ can be expressed as:

$$\frac{\sigma(\gamma_i\gamma_j)}{M(\gamma_i\gamma_j)} = \frac{1}{2}\sqrt{\frac{\sigma^2(E_i)}{E_i^2} + \frac{\sigma^2(E_j)}{E_j^2}}\,, \tag{3.2}$$

where E_i and E_j are the cluster energies, and $\sigma(E_i)$ and $\sigma(E_j)$ are their respective energy resolutions. We require the value of $\chi^2(2\pi^0)$ for the best combination to be greater than 2.6. This threshold has been optimised to reduce the contribution from events with two π^0 mesons by 90%, while retaining 85% of the signal.

To suppress background from the $\eta \to 3\pi^0$ decay in events where two photons are lost, a dedicated kinematic fit is performed. In addition to the standard 9-constraint (9C) conditions, this fit incorporates characteristics of such events, specifically the total energy deposited in the EMC and the missing momentum. The hypothesis of the fit is the decay $\phi \to (\eta \to 3\pi^0)\gamma$, with energy and momentum conservation enforced.

The first step of the fitting procedure is to determine initial estimates for the momenta of the two lost photons. It is assumed that the missing four-momentum corresponds to the sum of the four-momenta of these photons, and that each pair of reconstructed photons originates from a different π^0 decay. Cases in which an entire π^0 meson is lost are accounted for by the 11-constraint (11C) kinematic fit with two π^0 mass constraints. Under this assumption six constraints are provided, necessary to determine the two unknown momenta. A solution exists only if the invariant mass constructed from the missing four-momentum combined with the four-momenta of the two candidate partners of the missing photons exceeds $m(\pi^0)$. If no solution is found, the event is treated as one without two lost photons and retained for further analysis. If at least one valid solution is found, it is used as the initial value for the iterative kinematic fit. This procedure reduces the $\eta \to 3\pi^0$ background with two lost photons by 15% while preserving over 97% of the signal.

For the $\eta \to 3\pi^0$ case involving merged photons — where two photons share the same cluster — a Multivariate Data Analysis (MVA) method, Boosted Decision Trees (BDT) [24, 25], is employed. This technique utilises the properties of the clusters, including their energy and cell multiplicity, to discriminate between "normal" and "merged" clusters. The BDT is trained using signal $\eta \to \pi^0\gamma\gamma$ MC events and $\eta \to 3\pi^0$ MC events containing only merged clusters (i.e., five reconstructed clusters). Since the calorimeter has distinct structures in the endcaps and barrel, the BDT training is performed separately for these two regions according to the cluster position. Clusters comprising a single cell only are not considered. The training samples for both categories consisted of 5000 clusters each. The testing phase was conducted on an independent set of 5000 clusters for the normal and merged classes in both the barrel and endcaps. The cut-off values for the BDT response (-0.0365 for the barrel and -0.0136 for the endcaps) were chosen to maximise the significance, defined as $S/\sqrt{S+B}$, where S represents the signal (normal clusters) and B the background (merged clusters). The single-cluster efficiencies are 96.6% for the normal class and 20.3% for the merged class in the barrel, and 91.1% and 18.4%, respectively, in the endcaps. The BDT response is evaluated for all clusters within an event; if even one cluster is identified as merged, the entire event is rejected from the analysis. The test results for the barrel calorimeter clusters are presented in figure 3. Table 1 presents the number of events remaining after

JHEP01(2026)091

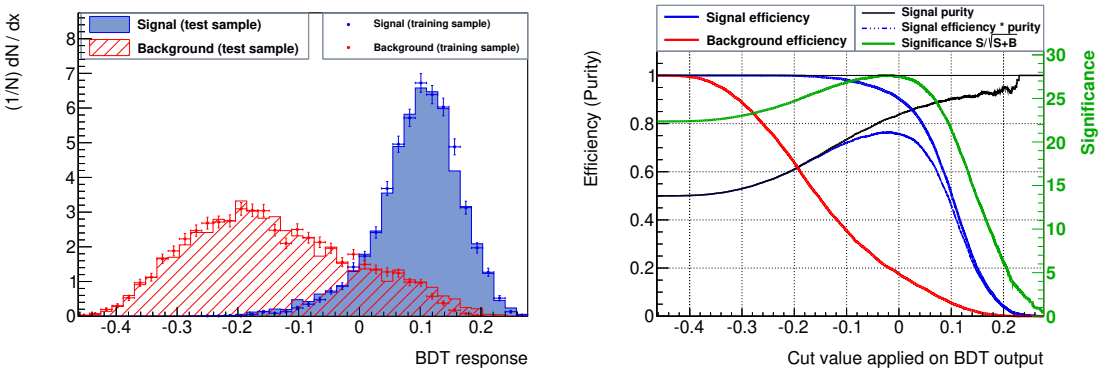


Figure 3. (**Left**) Comparison of the BDT response between the training samples (points with error bars) and independent test samples (solid histograms) for the EMC barrel, showing normal clusters in blue and merged clusters in red. (**Right**) Curves for signal (solid blue), background (red) efficiencies, and significance (solid green).

preselection, and those surviving all selection cuts.

To summarise, we select five prompt photons with a total energy sum exceeding 800 MeV. Each photon is required to have a polar angle between 25° and 155° and an energy above 20 MeV. Photon energies and times are corrected using a 9C kinematic fit, and events are retained if the fit probability exceeds 10%. Backgrounds from $\phi \to (a_0 \to \pi^0\eta)\gamma$, $\phi \to (f_0 \to \pi^0\pi^0)\gamma$, and $e^+e^- \to (\omega \to \pi^0\gamma)\pi^0$ are reduced by applying two 11C kinematic fits with a probability cut at 10%. Neutral pion pairs are further suppressed using a χ^2 cut at 2.6, while merged clusters are addressed via the BDT method. The number of selected data events is 45,698, with a final signal efficiency determined from MC simulation of $\epsilon_S = (15.45 \pm 0.09)\%$.

4 The normalisation channel

The decay $\eta \to 3\pi^0$ is chosen as the normalisation channel due to its similar topology and the well-known branching fraction value of $\mathcal{B}(\eta \to 3\pi^0) = \mathcal{B}_{3\pi^0} = (32.57 \pm 0.21)\%$ [5]. The selection criteria for the photons are identical to those used for the $\eta \to \pi^0\gamma\gamma$ signal extraction: minimum photon energies, polar angles, total deposited energy, and timing windows. To reject events involving photon splitting (i.e. when a single photon produces two separate clusters), we require that each pair of clusters has an opening angle greater than 18°. As with the signal, the resolution in energy and time is improved using an 11C kinematic fit, which imposes total energy-momentum conservation and time-of-flight constraints on the photons. A kinematic fit probability greater than 10% is required to suppress poorly reconstructed events. We exclude the recoil photon (the one closest to 363 MeV) and require the invariant mass of the six remaining photons to be consistent with the η meson mass. The efficiency for the $\eta \to 3\pi^0$ signal is $\epsilon_{3\pi^0} = (17.94 \pm 0.01)\%$, with backgrounds well below the 1% level. An unbinned three-component maximum likelihood fit is performed on the $M(3\pi^0)$ distribution, where the shapes of the $\eta \to 3\pi^0$ signal and backgrounds are taken from the MC simulation. The numbers of events for the subsamples consisting of 7 photons, or the combined samples of 6, 7, or 8 photons, are presented in table 2. For the 6γ and 8γ samples, $M(3\pi^0)$ is constructed

JHEP01(2026)091

Sample	N_{data} (10^3)	$N_{3\pi^0}$ (10^3)	N_{bckg} (10^3)	$\epsilon_{3\pi^0}(\%)$	N_{norm} (10^6)
7γ	4805	4791	14	17.94 ± 0.01	81.98 ± 0.53
6, 7 or 8γ	7125	7079	46	27.12 ± 0.01	80.15 ± 0.52

Table 2. Number of events selected for $\eta \to 3\pi^0$, number of background events, $\eta \to 3\pi^0$ efficiency, and the corresponding number of η mesons produced for the two samples: 7γ and the combined 6γ, 7γ, or 8γ, as determined after the fit. The uncertainties are statistical only.

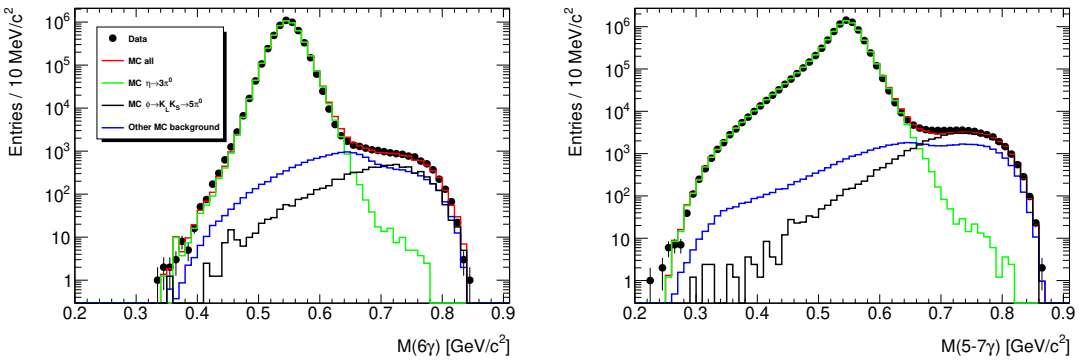


Figure 4. Distributions of $M(6\gamma)$ (**left**) and $M(5\text{–}7\gamma)$ (**right**), with a logarithmic scale on the Y-axis, shown after the fit. Data are represented by black points with error bars; the red histogram is the sum of all MC contributions: green histogram — $\eta \to 3\pi^0$ signal; black histogram — $\phi \to K_S K_L \to 5\pi^0$ background; blue histogram — all other background contributions.

using 5 and 7 photons, respectively. The main residual backgrounds after selection arise from $\phi \to K_S K_L \to (2\pi^0)(3\pi^0)$ and $\phi \to (\eta' \to \eta\pi^0\pi^0)\gamma$, with the subsequent decay $\eta \to \gamma\gamma$. The distributions of the invariant masses of 6 and 5–7 photons are shown in figure 4, for the 7-photon subsample and for the combined 6-, 7-, and 8-photon subsamples. The corresponding number of η mesons produced (N_{norm}) is calculated using the 7-photon sample. For the systematic uncertainty study, three sources are considered: cluster merging, photon splitting, and the analysis cut on the kinematic fit probability. The first two systematic uncertainties are estimated using the 6-, 7-, and 8-photon subsamples, by taking half of the difference from the 7-photon N_{norm} measurement, resulting in a 1.1% uncertainty. The uncertainty associated with the kinematic fit probability cut is evaluated by varying its value by 5% around the nominal value, yielding a systematic uncertainty of 0.6%. Additionally, the uncertainty on the $\mathcal{B}_{3\pi^0}$ value is included. The total systematic uncertainty of 1.4% is obtained by summing the individual contributions in quadrature, assuming all sources are independent. The final calculated number of η mesons is: $N_{\text{norm}} = N_{3\pi^0}/\epsilon_{3\pi^0}/\mathcal{B}_{3\pi^0} = (81.98 \pm 0.53_{\text{stat}} \pm 1.16_{\text{syst}}) \times 10^6$.

5 The signal extraction

To determine the number of signal events, we perform an unbinned three-component maximum likelihood fit to the $M(\pi^0\gamma\gamma)$ distribution. In this fit, the signal and background shapes are taken from the MC simulation, with all non-peaking backgrounds from the a_0, f_0, and ω decays combined. In the MC, $\phi \to \eta\gamma$ is generated according to its known production cross-section of 3 μb, while the production cross-sections and decay ratios for the a_0, f_0, and

JHEP01(2026)091

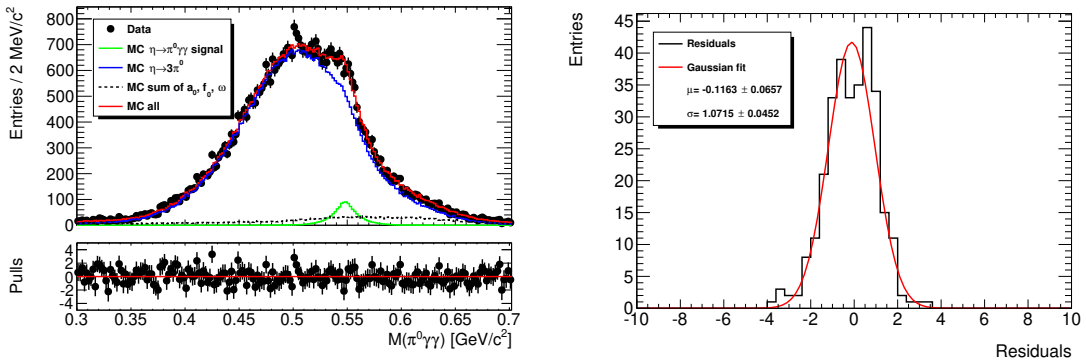


Figure 5. (**Left**) Result of the fit to the $M(\pi^0\gamma\gamma)$ distribution. Data are shown as black points with error bars; the red histogram represents the sum of all MC contributions. The green line indicates the $\eta \to \pi^0\gamma\gamma$ signal, the blue line corresponds to the $\eta \to 3\pi^0$ background, and the dotted black line shows the combined contribution from the a_0, f_0, and ω channels. The residuals are displayed below the main distribution. (**Right**) Distribution of residuals with a superimposed Gaussian fit (red line); the fitted Gaussian parameters with their statistical uncertainties are given in the box.

		Correlation coefficient	
Fit component	Yield	$\eta \to 3\pi^0$ background	Non-$3\pi^0$ background
$\eta \to \pi^0\gamma\gamma$ signal	1246 ± 133	-0.40	-0.02
$\eta \to 3\pi^0$ background	45232 ± 307		-0.52
Non-$3\pi^0$ background	3546 ± 190		

Table 3. Results of the three-component fit with statistical uncertainties and the corresponding correlation coefficients.

ω are taken from the corresponding KLOE results [19–23]. The invariant mass $M(\pi^0\gamma\gamma)$ is calculated by excluding the photon whose energy is closest to 363 MeV, corresponding to the recoil photon from the $\phi \to \eta\gamma$ decay. The χ^2 test of the fit yields $\chi^2/\text{n.d.f.} = 215/200$, where n.d.f. denotes the number of degrees of freedom, corresponding to a p-value of 22%. The fit results are shown in figure 5. The numbers of events for each component obtained from the fit, including their statistical uncertainties and correlation coefficients, are reported in table 3.

The branching fraction $\mathcal{B}(\eta \to \pi^0\gamma\gamma)$ is calculated as:

$$\mathcal{B}(\eta \to \pi^0\gamma\gamma) = \frac{N_S}{N_{\text{norm}}}\frac{1}{\epsilon_S} = \frac{N_S}{N_{3\pi^0}}\frac{\epsilon_{3\pi^0}}{\epsilon_S}\mathcal{B}_{3\pi^0}, \tag{5.1}$$

where N_S denotes the number of signal events obtained from the fit, ϵ_S is the signal efficiency determined from the MC simulation, and N_{norm} is the final number of η mesons. The resulting branching fraction is $\mathcal{B}(\eta \to \pi^0\gamma\gamma) = (0.98 \pm 0.11) \times 10^{-4}$, where the uncertainty is statistical only.

To measure the decay rate as a function of the invariant mass squared, $M^2(\gamma\gamma)$, of the two bachelor photons (i.e. those not originating from the π^0 decay), the data are divided into seven bins of $M^2(\gamma\gamma)$. The bin ranges are: 1^{st} : $(0, 0.011)$, 2^{nd} : $(0.0275, 0.0475)$, 3^{rd} : $(0.0475, 0.0675)$, 4^{th} : $(0.0675, 0.0875)$, 5^{th} : $(0.0875, 0.1075)$, 6^{th} : $(0.1075, 0.13)$, and 7^{th} : $(0.13, 0.17)$ in units of GeV^2/c^4. These ranges are illustrated in figure 6 by the histogram

JHEP01(2026)091

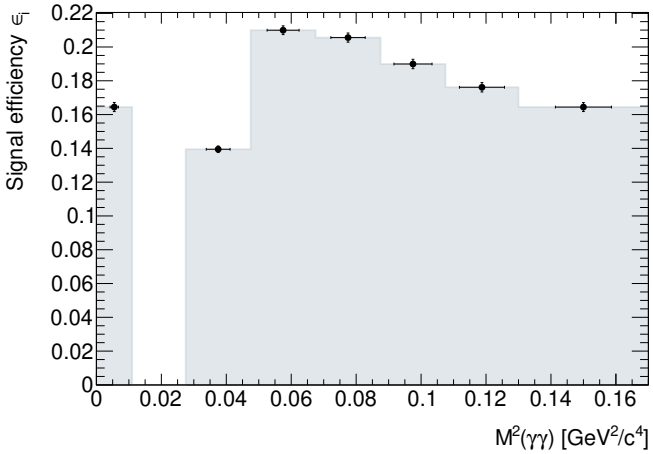


Figure 6. Detection efficiencies ϵ_i for $\eta \to \pi^0\gamma\gamma$ in bins of $M^2(\gamma\gamma)$, evaluated using MC simulation. The resolution in $M^2(\gamma\gamma)$ is shown as horizontal $\pm 1\sigma$ lines centred on each bin. Bin boundaries are indicated by the histogram bin widths. The region $(0.0110, 0.0275)\,\mathrm{GeV}^2/\mathrm{c}^4$ is excluded due to the $\pi^0\pi^0$ veto.

of the detection efficiency in each bin. The region close to the neutral pion mass squared, $(0.0110, 0.0275)\,\mathrm{GeV}^2/\mathrm{c}^4$, is excluded since events in this interval are removed by the veto on $\pi^0\pi^0$ pairs. The corresponding bin efficiencies shown in figure 6 are derived from the signal MC sample generated with a constant matrix element for $\eta \to \pi^0\gamma\gamma$. The efficiency for the i-th bin, ϵ_i, is defined as the ratio of events reconstructed within that bin to the number of events generated with $M^2(\gamma\gamma)$ values falling within the bin limits. The number of events in each $M^2(\gamma\gamma)$ bin is determined using the same fitting procedure as for the branching fraction measurement, applied separately to each bin. The results are shown in figure 7. The decay width $d\Gamma(\eta \to \pi^0\gamma\gamma)/dM^2(\gamma\gamma)$ is then calculated as

$$\left.\frac{d\Gamma}{dM^2}\right|_i = \frac{N_S^{(i)}}{\epsilon_S^{(i)} \cdot N_{\mathrm{norm}}} \frac{\Gamma}{w_i}\,, \tag{5.2}$$

where $N_S^{(i)}$ is the signal yield in the i-th bin, w_i is the width of the bin, $\epsilon_S^{(i)}$ is the signal efficiency for the bin, N_{norm} is the total number of η mesons, and $\Gamma = (1.31 \pm 0.05)\,\mathrm{keV}$ is the full width of the η meson [5]. The statistical uncertainties correspond to those of $N_S^{(i)}$ obtained from the fit. The sum of $N_S^{(i)}$ is $1262 \pm 140_{\mathrm{stat}}$, in good agreement with the total signal yield of $1246 \pm 133_{\mathrm{stat}}$.

6 Systematic studies

The systematic effects considered include trigger conditions, background filter, data streaming, consistency between data acquisition periods within the analysis sample, photon counting efficiency, identification of the recoil photon, selection cuts applied in the analysis, biases in the fitting procedure, normalisation error, signal MC model, and finally the effect of data-MC discrepancies observed in the low $M(\gamma\gamma)$ region (below 25 MeV). For $d\Gamma/dM^2$, an additional

JHEP01(2026)091

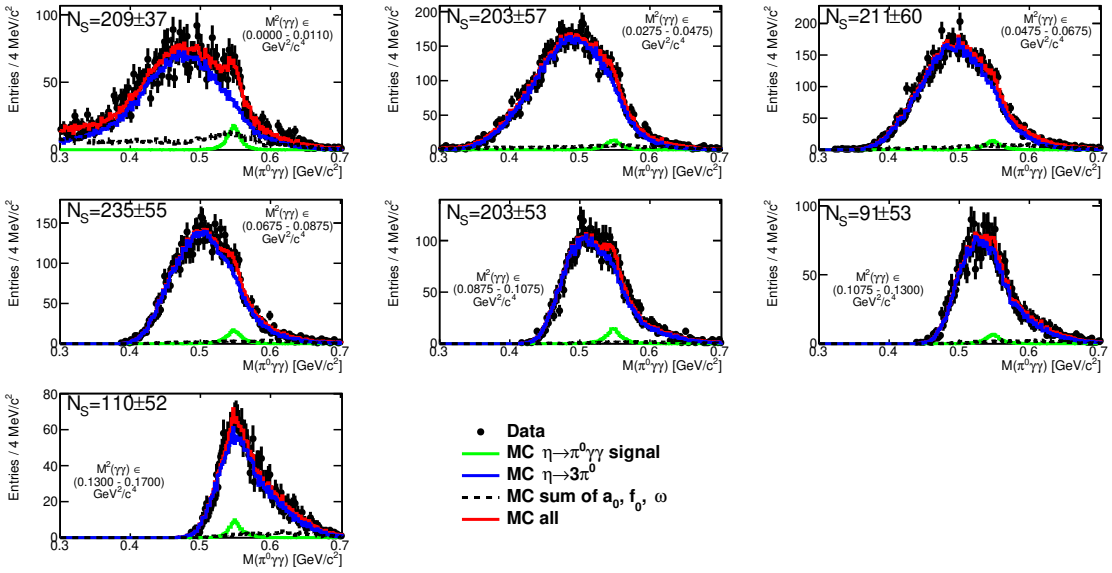


Figure 7. Fits to the $M(\pi^0\gamma\gamma)$ distributions for each $M^2(\gamma\gamma)$ bin, as shown in figure 5 (left). The text in the upper-left corner indicates the number of $\eta \to \pi^0\gamma\gamma$ signal events extracted from the fits. The $M^2(\gamma\gamma)$ bin ranges are displayed on the distributions.

uncertainty arising from the incorrect assignment of photons as originating from the π^0 decay is also taken into account. The systematic uncertainties are summarised in table 4.

The systematic effect arising from the trigger conditions was investigated using the MC simulated signal sample and found to be negligible. To estimate the systematic uncertainties due to the background filter and data streaming procedures, a data sample collected without streaming or background filtering was used, scaled down by a factor of ten. The resulting systematic uncertainty is estimated to be 1% for each effect. However, since our measurement normalises to a channel collected with exactly the same trigger during the same time period — meaning both the signal and $\eta \to 3\pi^0$ events are in the same data stream under the same background filter — the effects of trigger, background filter, and data streaming largely cancel out in the branching fraction and $d\Gamma/dM^2$ measurements.

Since the sample originates from two distinct data acquisition periods, we have verified that the results obtained from each period separately are consistent within the uncertainties.

The systematic uncertainty arising from the event selection is evaluated by varying each selection cut independently within its own resolution. Half of the difference between the maximum and minimum results obtained for each cut is taken as the estimate of the systematic uncertainty. The total uncertainty is then calculated as the quadratic sum of the individual contributions, assuming all sources are independent.

To estimate the systematic uncertainty arising from the pairing procedure used in the analysis, the $\eta \to \pi^0\gamma\gamma$ sample is studied using the MC-generated signal by matching the generated photon pairs to the selected π^0 candidates and to the unpaired photons. According to MC studies, the fraction of events with incorrectly combined photons is 5.1%. An alternative fit is performed by excluding these wrongly combined events from the MC signal sample.

JHEP01(2026)091

The resulting change in the branching fraction is 0.6%, which is considered negligible. The difference between the two fit results for $d\Gamma/dM^2$ is taken as a source of systematic uncertainty.

The uncertainties related to the analysis conditions are assessed by sequentially varying each cut value within its own resolution. As all kinematic fits are correlated, the probability cut is varied separately for each fit. The maximum and minimum changes in the branching fraction and $d\Gamma/dM^2$ relative to the nominal results are then determined. Half of the difference between these maximum and minimum values, considered separately for each selection, is taken as the systematic uncertainty.

Different binning schemes of the $M(\pi^0\gamma\gamma)$ distribution and fitting ranges are employed to estimate the associated uncertainties. The resulting changes in the branching fraction and $d\Gamma/dM^2$ relative to the nominal values are found to be negligible. Resolution effects on the $d\Gamma/dM^2$ distribution have been studied using MC simulation, yielding negligible modifications to the distribution and insignificant impacts on the efficiency determinations within the chosen binning scheme.

The systematic uncertainty on the normalisation is estimated to be 1.4%, as detailed in section 4.

To estimate the systematic uncertainty arising from the MC model, the phase-space distribution of $M^2(\gamma\gamma)$ in $\eta \to \pi^0\gamma\gamma$ is replaced with the model proposed in ref. [6]. The resulting branching fraction and $d\Gamma/dM^2$ values are found to be consistent with those obtained in the nominal analysis.

For the $d\Gamma/dM^2$ analysis, we distinguish between uncertainties common to all points and those that are uncorrelated. For each statistical or systematic uncertainty, we subtract in quadrature from each $d\Gamma/dM^2$ bin the corresponding uncertainty derived from the branching fraction analysis. This common uncertainty amounts to 18.2%. The uncertainty arising from the finite MC statistics is negligible.

We observe a discrepancy between MC and data for $M(\gamma\gamma)$ values below 25 MeV, as shown in figure 8. Since both clusters are close in space and time, and one has significantly lower energy, these are attributed to photon splitting events originating from the $\phi \to \eta\gamma \to 3\gamma$, $\phi \to \pi^0\gamma \to 3\gamma$, or $e^+e^- \to \gamma\gamma$ processes. This effect is studied by applying cuts that remove events with $M(\gamma\gamma)$ less than 20, 25, 30, and 50 MeV. The extracted value of $d\Gamma/dM^2$ in the standard analysis for the first bin is $(1.96 \pm 0.37_{\text{stat}})\,\text{eV}/(\text{GeV}^2/\text{c}^4)$. By excluding events with small $M(\gamma\gamma)$, the largest observed change is $\Delta = 0.11\,\text{eV}/(\text{GeV}^2/\text{c}^4)$ for $M(\gamma\gamma) > 25\,\text{MeV}$, which corresponds to a negligible contribution compared to other systematic effects. Furthermore, the uncertainty of Δ, denoted $\sigma(\Delta)$, is calculated taking into account the correlation between the samples [26]. The ratio $\Delta/\sigma(\Delta) = 1.8$ indicates that this change can be interpreted as an insignificant systematic effect (see ref. [26]) on the value of $d\Gamma/dM^2$ in the first bin. The same checks performed on the branching fraction $\mathcal{B}(\eta \to \pi^0\gamma\gamma)$ yield similarly negligible effects.

The systematic uncertainties are summarised in table 4.

7 Results

Using a data sample of 1.7 fb^{-1}, corresponding to $(81.98 \pm 0.53_{\text{stat}} \pm 1.03_{\text{syst}}) \times 10^6$ η mesons, collected with the KLOE detector, 1246 ± 133 $\eta \to \pi^0\gamma\gamma$ events are selected from the

JHEP01(2026)091

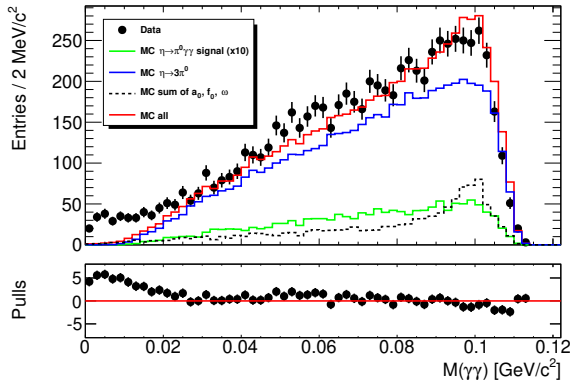


Figure 8. Small invariant mass region of non-π^0 photons. Data are shown as black points with error bars. The red histogram represents the sum of all MC contributions: the green line corresponds to the $\eta \to \pi^0\gamma\gamma$ signal (scaled up by a factor of 10), the blue line to the $\eta \to 3\pi^0 \to 5\gamma$ channel, and the dashed black line to the sum of the a_0, f_0 and ω channels. All MC distributions are normalised according to the results of the 3-component fit to $M(\pi^0\gamma\gamma)$. Residuals are shown below the distribution.

Source of uncertainty	$\mathcal{B}(\eta \to \pi^0\gamma\gamma)$	$d\Gamma/dM^2$ bin number						
		1^{st}	2^{nd}	3^{rd}	4^{th}	5^{th}	6^{th}	7^{th}
Preselection	11	38	11	17	19	1	56	34
Analysis cuts	9	27	42	25	21	10	46	41
Photon pairing	0.6	2	4	1	1	4	2	8
Normalisation	1	1	1	1	1	1	1	1
Total	14	46	44	30	28	10	73	54

Table 4. The relative systematic uncertainties of the branching fraction $\mathcal{B}(\eta \to \pi^0\gamma\gamma)$ and of all bins of the differential decay width $d\Gamma(\eta \to \pi^0\gamma\gamma)/dM^2(\gamma\gamma)$ are given in %. The effects of fitting bias, MC model, small $M(\gamma\gamma)$ values, and run period result in negligible contributions to the systematic uncertainty.

$\phi \to \eta\gamma$ radiative decays. The branching fraction of the $\eta \to \pi^0\gamma\gamma$ process is measured to be $\mathcal{B}(\eta \to \pi^0\gamma\gamma) = (0.98 \pm 0.11_{\text{stat}} \pm 0.14_{\text{syst}}) \times 10^{-4}$. This value is approximately a factor of two smaller than the recent experimental measurements reported in refs. [10, 11], and confirms the preliminary result from KLOE [12]. Our result is consistent with the recent theoretical calculation presented in [6], which predicts $\mathcal{B} = (1.30 \pm 0.08) \times 10^{-4}$. Using the full width of the η meson, $\Gamma = (1.31 \pm 0.05)$ keV [5], the partial decay width is $\Gamma(\eta \to \pi^0\gamma\gamma) = (0.13 \pm 0.02)$ eV, where the uncertainty is the quadratic sum of the PDG value and our measurement.

The results for the differential decay width distribution, $d\Gamma(\eta \to \pi^0\gamma\gamma)/dM^2(\gamma\gamma)$, are presented in figure 9 and summarised in table 5. The systematic uncertainties include the contributions listed in table 4. These errors are partially correlated, with a portion of the uncertainty common to all data points. This common contribution, estimated from the uncertainty of the branching fraction value, is treated separately, subtracted from all points, and shown as a grey band in figure 9. In the same figure, our results are compared with previous measurements from refs. [10, 11], and with theoretical predictions from refs. [3, 4, 6].

JHEP01(2026)091

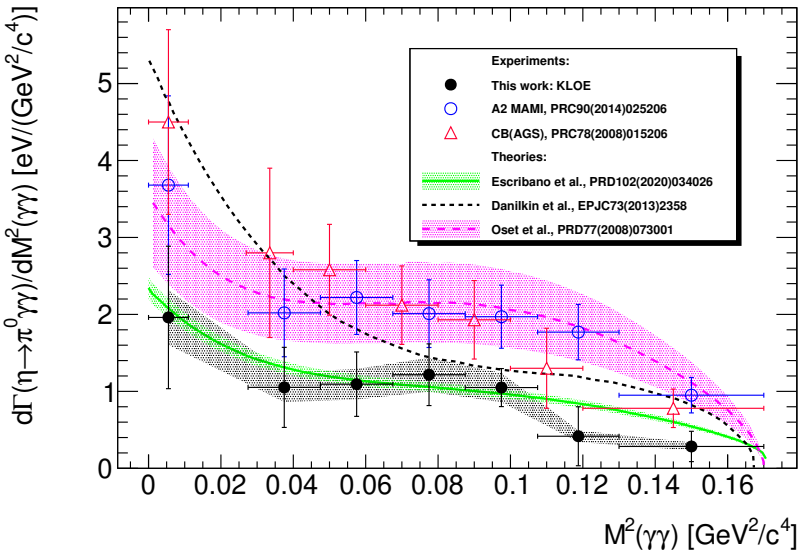


Figure 9. Measured differential decay width distribution, $d\Gamma(\eta \to \pi^0\gamma\gamma)/dM^2(\gamma\gamma)$ (black points with error bars; grey band indicates the common systematic uncertainty), compared with previous experimental results: red triangles from ref. [10] and blue circles from ref. [11]. All uncertainties on $d\Gamma/dM^2$ are total errors. The data are also compared with theoretical predictions from ref. [6] (green solid line with shaded error band), ref. [3] (black dotted line), and ref. [4] (magenta dashed line with shaded error band).

Bin	1^{st}	2^{nd}	3^{rd}	4^{th}	5^{th}	6^{th}	7^{th}
Value [eV/(GeV^2/c^4)]	1.96	1.05	1.09	1.22	1.05	0.42	0.28
Statistical uncertainty (%)	14.7	26.1	26.6	21.3	24.5	57.2	46.2
Systematic uncertainty (%)	46.4	43.8	29.9	27.7	10.3	73.0	53.7
Total uncorrelated uncertainty (%)	48.7	51.0	40.0	35.0	26.6	92.7	70.9
Total common uncertainty (%)	18.2	18.2	18.2	18.2	18.2	18.2	18.2

Table 5. Values and relative uncertainties of the $d\Gamma(\eta \to \pi^0\gamma\gamma)/dM^2(\gamma\gamma)$ distribution. The bin ranges are: 1^{st} : $(0, 0.011)$, 2^{nd} : $(0.0275, 0.0475)$, 3^{rd} : $(0.0475, 0.0675)$, 4^{th} : $(0.0675, 0.0875)$, 5^{th} : $(0.0875, 0.1075)$, 6^{th} : $(0.1075, 0.13)$, 7^{th} : $(0.13, 0.17)$, all in GeV^2/c^4 units.

The branching fraction value obtained by integrating the $d\Gamma/dM^2$ distribution and normalising to the $\eta \to 3\pi^0$ channel is $\mathcal{B}(\eta \to \pi^0\gamma\gamma) = (1.00 \pm 0.11_{\text{stat}}) \times 10^{-4}$, which is in good agreement with the value obtained from the fit to the full distribution.

Acknowledgments

We warmly thank our former KLOE colleagues for the access to the data collected during the KLOE data taking campaign. We thank the DAΦNE team for their efforts in maintaining good running conditions and their collaboration during both the KLOE run [27] and the KLOE-2 data taking with an upgraded collision scheme [28, 29]. We are very grateful to our colleague G. Capon for his enlightening comments and suggestions about the manuscript. We

JHEP01(2026)091

want to thank our technical staff: M. Anelli for his continuous attention to the gas system and detector safety; A. Balla, M. Gatta, G. Corradi and G. Papalino for electronics maintenance; C. Piscitelli for his help during major maintenance periods. We sincerely thank the technical staff of the LNF computing and web service, S. Angius, R. Orrù, D. Spigone, and M. Tota, for their support in the maintenance of the KLOE Computing Center. We would like to express our gratitude to M. Pistoni for his help and technical support on computing, L. dell'Agnello, D. Cesini, and C. Pellegrino for their support in the KLOE/KLOE-2 data transfer at CNAF, A. Antonelli and M. Palutan, for their support while heading the LNF research division.

This work was supported in part by the Polish National Science Centre through the Grant No. 2017/26/M/ST2/00697 and the "Leverhulme Trust LIP-2021-014".

Data Availability Statement. This article has no associated data or the data will not be deposited.

Code Availability Statement. This article has no associated code or the code will not be deposited.

Open Access. This article is distributed under the terms of the Creative Commons Attribution License (CC-BY4.0), which permits any use, distribution and reproduction in any medium, provided the original author(s) and source are credited.

References

[1] B.R. Holstein, *Allowed η decay modes and chiral symmetry*, *Phys. Scripta T* **99** (2002) 55 [hep-ph/0112150] [INSPIRE].

[2] E. Oset, J.R. Pelaez and L. Roca, $\eta \to \pi^0\gamma\gamma$ *decay within a chiral unitary approach*, *Phys. Rev. D* **67** (2003) 073013 [hep-ph/0210282] [INSPIRE].

[3] I.V. Danilkin, M.F.M. Lutz, S. Leupold and C. Terschlusen, *Photon-fusion reactions from the chiral Lagrangian with dynamical light vector mesons*, *Eur. Phys. J. C* **73** (2013) 2358 [arXiv:1211.1503] [INSPIRE].

[4] E. Oset, J.R. Pelaez and L. Roca, $\eta \to \pi^0\gamma\gamma$ *decay within a chiral unitary approach revisited*, *Phys. Rev. D* **77** (2008) 073001 [arXiv:0801.2633] [INSPIRE].

[5] Particle Data Group collaboration, *Review of particle physics*, *Phys. Rev. D* **110** (2024) 030001 [INSPIRE].

[6] R. Escribano, S. Gonzàlez-Solís, R. Jora and E. Royo, *Theoretical analysis of the doubly radiative decays $\eta^{(\prime)} \to \pi^0\gamma\gamma$ and $\eta' \to \eta\gamma\gamma$*, *Phys. Rev. D* **102** (2020) 034026 [arXiv:1812.08454] [INSPIRE].

[7] I. Danilkin, O. Deineka and M. Vanderhaeghen, *Theoretical analysis of the $\gamma\gamma \to \pi^0\eta$ process*, *Phys. Rev. D* **96** (2017) 114018 [arXiv:1709.08595] [INSPIRE].

[8] J. Lu and B. Moussallam, *The $\pi\eta$ interaction and a_0 resonances in photon-photon scattering*, *Eur. Phys. J. C* **80** (2020) 436 [arXiv:2002.04441] [INSPIRE].

[9] L. Gan, B. Kubis, E. Passemar and S. Tulin, *Precision tests of fundamental physics with η and η' mesons*, *Phys. Rept.* **945** (2022) 1 [arXiv:2007.00664] [INSPIRE].

JHEP01(2026)091

[10] S. Prakhov et al., *Measurement of the invariant-mass spectrum for the two photons from the $\eta \to \pi^0\gamma\gamma$ decay*, *Phys. Rev. C* **78** (2008) 015206 [INSPIRE].

[11] A2 AT MAMI collaboration, *New measurement of the rare decay $\eta \to \pi^0\gamma\gamma$ with the Crystal Ball/TAPS detectors at the Mainz Microtron*, *Phys. Rev. C* **90** (2014) 025206 [arXiv:1405.4904] [INSPIRE].

[12] KLOE collaboration, *The $\eta \to \pi^0\gamma\gamma$, η/η' mixing angle and the η mass measurement at KLOE*, *Acta Phys. Slov.* **56** (2006) 403 [INSPIRE].

[13] DAFNE collaboration, *DAFNE status and upgrade plans*, *Phys. Part. Nucl. Lett.* **5** (2008) 560 [arXiv:0709.3696] [INSPIRE].

[14] KLOE collaboration, *Precision Kaon and Hadron Physics with KLOE*, *Riv. Nuovo Cim.* **31** (2008) 531 [arXiv:0811.1929] [INSPIRE].

[15] M. Adinolfi et al., *The tracking detector of the KLOE experiment*, *Nucl. Instrum. Meth. A* **488** (2002) 51 [INSPIRE].

[16] M. Adinolfi et al., *The KLOE electromagnetic calorimeter*, *Nucl. Instrum. Meth. A* **482** (2002) 364 [INSPIRE].

[17] KLOE collaboration, *The trigger system of the KLOE experiment*, *Nucl. Instrum. Meth. A* **492** (2002) 134 [INSPIRE].

[18] F. Ambrosino et al., *Data handling, reconstruction, and simulation for the KLOE experiment*, *Nucl. Instrum. Meth. A* **534** (2004) 403 [physics/0404100] [INSPIRE].

[19] KLOE collaboration, *Study of the decay $\phi \to \eta\pi^0\gamma$ with the KLOE detector*, *Phys. Lett. B* **536** (2002) 209 [hep-ex/0204012] [INSPIRE].

[20] KLOE collaboration, *Study of the $a_0(980)$ meson via the radiative decay $\phi \to \eta\pi^0\gamma$ with the KLOE detector*, *Phys. Lett. B* **681** (2009) 5 [arXiv:0904.2539] [INSPIRE].

[21] KLOE collaboration, *Study of the decay $\phi \to \pi^0\pi^0\gamma$ with the KLOE detector*, *Phys. Lett. B* **537** (2002) 21 [hep-ex/0204013] [INSPIRE].

[22] KLOE collaboration, *Dalitz plot analysis of $e^+e^- \to \pi^0\pi^0\gamma$ events at $\sqrt{s}$ approximately M(ϕ) with the KLOE detector*, *Eur. Phys. J. C* **49** (2007) 473 [hep-ex/0609009] [INSPIRE].

[23] KLOE collaboration, *Study of the process $e^+e^- \to \omega\pi^0$ in the ϕ-meson mass region with the KLOE detector*, *Phys. Lett. B* **669** (2008) 223 [arXiv:0807.4909] [INSPIRE].

[24] TMVA collaboration, *TMVA — Toolkit for Multivariate Data Analysis*, physics/0703039 [INSPIRE].

[25] H. Voss, A. Hocker, J. Stelzer and F. Tegenfeldt, *TMVA, the Toolkit for Multivariate Data Analysis with ROOT*, *PoS* **ACAT** (2007) 040 [INSPIRE].

[26] R. Barlow, *Systematic errors: Facts and fictions*, in the proceedings of the *Conference on Advanced Statistical Techniques in Particle Physics*, Durham, U.K., March 18–22 (2002) [hep-ex/0207026] [INSPIRE].

[27] A. Gallo et al., *DAFNE status report*, *Conf. Proc. C* **060626** (2006) 604 [INSPIRE].

[28] M. Zobov et al., *Test of crab-waist collisions at DAFNE Phi factory*, *Phys. Rev. Lett.* **104** (2010) 174801 [INSPIRE].

[29] C. Milardi, M.A. Preger, P. Raimondi and F. Sgamma, *High luminosity interaction region design for collisions inside high field detector solenoid*, 2012 *JINST* **7** T03002 [arXiv:1110.3212] [INSPIRE].

JHEP01(2026)091